Electronic Supplementary Material (ESI) for Environmental Science: Nano

Silk nanofibers-ZIF hybrid membrane with improved treatment efficiency and highly enhanced water permeability for excellent removal of multiple pollutants in water

Dina Sun, Gengping Meng, Shihao Sun, Wenting Guo, Jun Hai, Junxia Su, Yanxia Song, Fengjuan Chen*, Baodui Wang**

State Key Laboratory of Applied Organic Chemistry and Key Laboratory of Nonferrous Metal Chemistry and Resources Utilization of Gansu Province, Lanzhou University, Lanzhou, 730000,

P. R. China

*Email: haij@lzu.edu.cn; chenfj@lzu.edu.cn; wangbd@lzu.edu.cn

Experimental section.

Materials and Chemicals. All reagents and solvents were obtained commercially and used without further purification unless otherwise noted. Silk cocoons were purchased from the Alibaba Group and factory wastewater used in the experiment from a sewage treatment plant (Jinchuan Group Ltd., China). Zinc nitrate hexahydrate ($Zn(NO_3)_2 \cdot 6H_2O$, 98%), copper sulfate ($CuSO_4$), lead acetate ($Pb(Ac)_2$), cadmium nitrate ($Cd(NO_3)_2$), mercuric acetate ($Hg(Ac)_2$), hydrochloric acid (HCl, 37%), sodium carbonate (Na_2CO_3), sodium sulfate (Na_2SO_4), sodium nitrite ($NaNO_2$), sodium hydroxide (NaOH), and ethanol (EtOH, ≥99.7%) were provided by Lianlong Tianjin Pharmaceutical Chemical Co. Ltd. Lithium bromide (LiBr), 2-methylimidazole (Hmim, 99%), Congo red, rhodamine B and methylene blue were from Aladdin reagents. Deionized (DI) water was used in all experiments.

Characterizations. The structural details of SNFs were characterized by transmission electron microscope (TEM, FEI, Talos 200s). The morphology of SNFs-ZIF membrane was imaged by using a field emission scanning electron microscope (FE-SEM, FEI, Sirion 200). The chemical properties of the SNFs-ZIF were characterized by Fourier transform infrared spectrometer (FI-IR, Nicolet, FT-170SX), X-ray powder diffraction (XRD, AXS D8-Advanced diffractometer) and X-ray photoelectron spectroscopy (XPS, a PHI5702 multifunctional spectrometer). An energy-dispersive X-ray (EDX) spec

troscope attached to the FE-SEM was utilized to analyze the element distributions in the cross section of SNFs-ZIF. UV−vis absorbance measurements (UV-vis, Shimadzu, UV-1750) were used to evaluate the treatment efficiency for organic dyes of the membrane and the content of NO_2^--N and NH_4^+-N in wastewater. The concentrations of Cu^{2+}, Pb^{2+}, Pd^{2+} and Cd^{2+} in water were measured by inductively coupled plasma mass spectrometry (ICP-MS, PerkinElmer Elan DRC II). While, Hg^{2+} was measured by atomic fluorescence spectroscopy (AFS). Electrochemical properties of the carbonized membrane were tested by an electrochemical station (CHI760E, Shanghai Chenhua Ltd.). Ion Chromatography (ICG, 1500) was used to determine the content of NO_3^--N in wastewater.

Filtration Experiments.

All filtration experiments are carried out in a filter device with an effective membrane area of 12 cm^2 and a pressure of 0.8 0.8 bar^{-1}. The schematic diagram of SNFs-ZIF hybrid membranes fabrication is depicted in Figure S1. The SNFs-ZIF hybrid membranes were further obtained by depositing SNFs-ZIF dispersions on PC substrate through vacuum-assisted filtration. Several kinds of typical heavy metal ions in industrial wastewater were selected to evaluate the removal performance of the SNFs-ZIF hybrid membranes, including Cu^{2+}, Pb^{2+}, Cd^{2+} and Hg^{2+}, which were prepared by dissolving $CuSO_4$, $Pb(Ac)_2$, $Cd(NO_3)_2$ and $Hg(Ac)_2$ salts in DI water, respectively. The ion concentration was measured by ICP-MS and AFS, then the removal efficiency was calculated according to the formula (1):

$$\text{Removal efficiency (\%)} = 100\times(C_0\text{-}C)/C_0 \quad (1)$$

where C_0 and C are the concentrations of metal ions before and after the SNFs-ZIF hybrid membranes treatment, respectively. Water flux was calculated according to formula (2)

$$Q = V/(T\times A\times P) \quad (2)$$

Among them, V is the volume of treated solution (L), T is the time of solution flowing through the membrane (h), A is the effective area (m^2) of the membrane, and P is the operating pressure (bar). Q represents water flux at unit pressure ($L\cdot m^{-2}\cdot h^{-1}\cdot bar^{-1}$). The analysis method of the actual sample of factory wastewater after membrane filtration is consistent with the solution prepared in the laboratory. Additionally, congo red, rhodamine B and methylene blue were dissolved in DI water (50 ppm) to evaluate the performance of the membrane for removing organic dyes from wastewater. The contents of three organic dyes in the water before and after filtration were determined by UV-vis spectroscopy.

Preparation of composite Electrode. Thermal reduction process was employed to reduce the palladium ions into the nanoparticles whilst converting the SNFs-ZIF membrane into the carbonized membrane (CM). The membrane (105 μm) with protein content of 6.7wt % was utilized for vacuum-assisted filtration of 0.5 M $PdCl_2$ solution (50 mL). Then, the film containing $PdCl_2$ was dried in an oven at 40 ℃ for 12 h. Pd/CM powder was obtained by calcining the dried film at 500 ℃ for 3 h in a tubular furnace.

Next, 10 μL nafion solution was added into 2 mg·mL^{-1} Pd/CM suspension (2 mL) to make the composite easy to deposit on carbon paper (CP, 1.0 cm × 1.0 cm). Pd/CM suspension of 250 μL was drawn to deposit on both sides of carbon paper, which was finally fastened in glassy carbon electrode (GCE) clamp for as working electrode.

Electrocatalytic Reduction of NO_3^--N. Composite electrodes (1.0 cm × 1.0 cm), platinum sheet (1.0 cm × 1.0 cm) and saturated calomel electrodes were used in an electrochemical cell divided with a proton exchange membrane as the working electrode, counter electrode, and reference electrode, respectively. The working electrode was prepared by mixing 2 mg·mL^{-1} catalyst (dispersed in mixed solvent of ethanol and DI water) and 0.5% Nafion solution to form a homogeneous dispersion. The dispersion (500 μL) was then modified the carbon paper (1 × 1 cm) by drop-coating which was acted as the cathode. The cathode cells contained 27 mL of 0.5 mol·L^{-1} Na_2SO_4 and 3 mL sodium nitrate stock solution (50 mg·L^{-1} NO_3^--N), while anode cells contained 30 mL·Na_2SO_4 (0.5 mol·L^{-1}). Electrocatalytic reduction of NO_3^--N tests were performed on a CHI 760E electrochemical analyzer system at −1.3 V (vs. SCE) for 60 h. The nitrate conversion was calculated by the equations (3):

$$\text{Conversion (\%)} = (C_0 - C_t)/ C_0 \times 100 \quad (3)$$

Where C_0 is the initial concentration (mg·L^{-1}) of NO_3^--N, C_t is the concentration (mg·L^{-1}) of NO_3^--N at time t. The nitrate removal capacity was used to evaluate the

catalytic activity in unit weight of the material, which was calculated using the following equation:

$$RC = (C_0 - C_t)\ V/m \quad (4)$$

where V (L) is the volume of the nitrate solution and m (g) is the mass of nanocomposites coated on carbon papers. The selectivity for N_2 was evaluated using the equation (5):

$$S\ (\%) = \frac{\Delta(NO3^- - N) - \Delta(NH4^+ - N) - \Delta(NO2^- - N)}{\Delta(NO3^- - N)} \times 100 \quad (5)$$

where $\Delta(NO3^- - N)$, $\Delta(NH4^+ - N)$, and $\Delta(NO2^- - N)$ are the changes of nitrate, ammonium and nitrite concentration before and after the reaction, respectively. Energy consumption (EC) was determined according to the equation (6):

$$EC = \frac{VAt}{J\Delta(NO3^- - N)} \times 10 - 3 \quad (6)$$

Among them, V stands for potential (V), I is the current (A), and J is the volume of the solution (m^3).

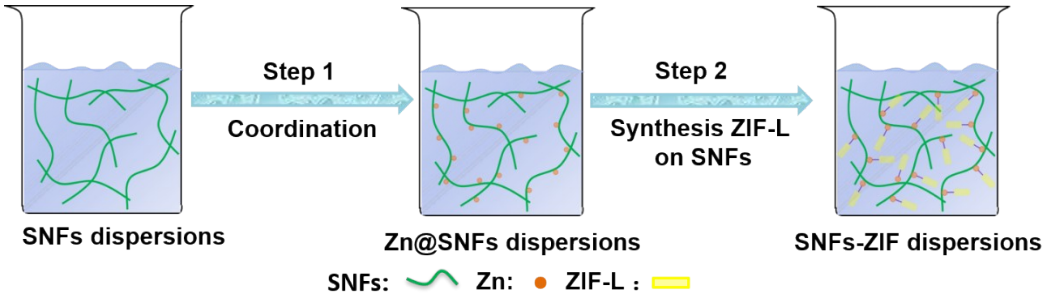

Figure S1. Diagrammatic sketch of the synthesis of SNFs-ZIF hybrid materials.

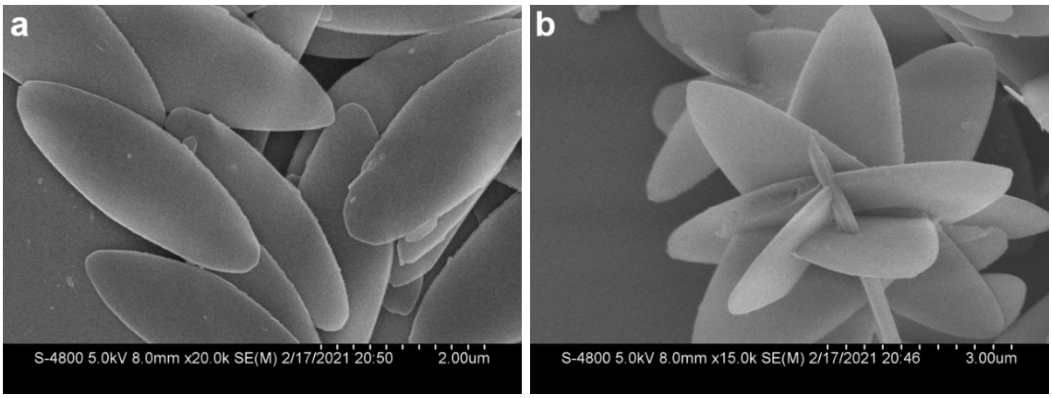

Figure S2. SEM images of typical ZIF-L crystals: (a) top view image showing leaf-like shape and (b) side view image indicating the crystal thickness.

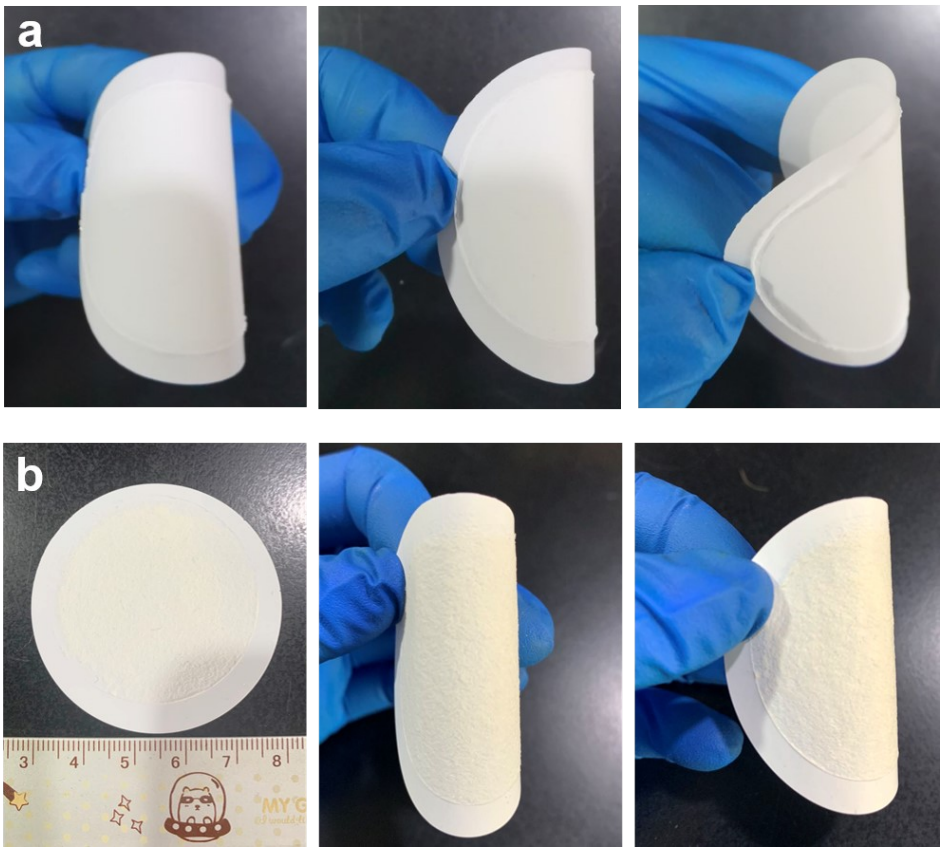

Figure S3. (a) The photos of the SNFs-ZIF hybrid membrane, indicating the film can bend freely without cracks. (b) The photos of the pure SNFs membrane demonstrate the discontinuous fluffy particles in surface, which are easily broken.

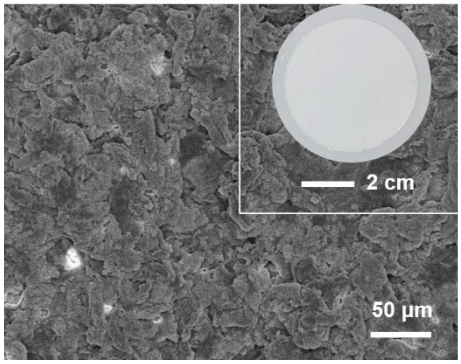

Figure S4. SEM image of the membrane surface. Insert: the macrophotograph of membrane surface.

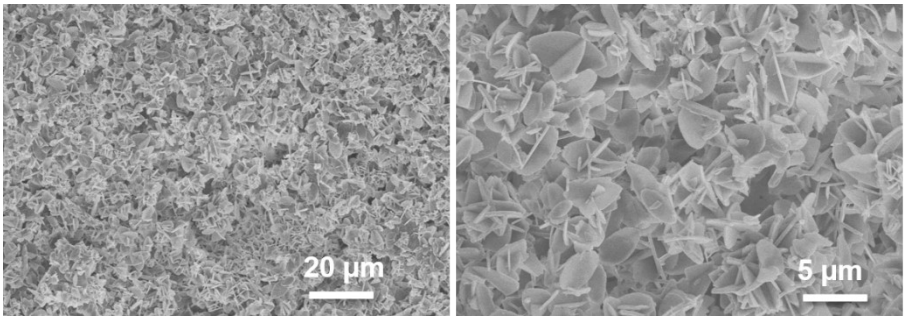

Figure S5. SEM images of the SNFs-ZIF hybrid material.

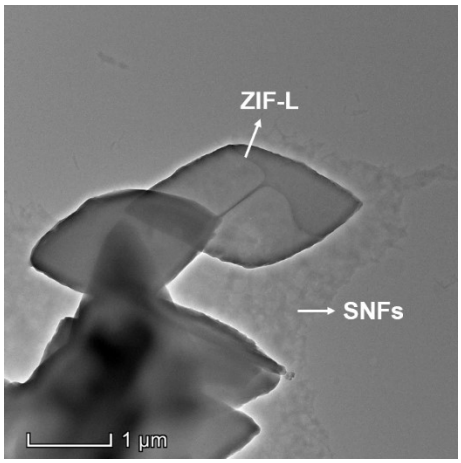

Figure S6. TEM images of the SNFs-ZIF hybrid material.

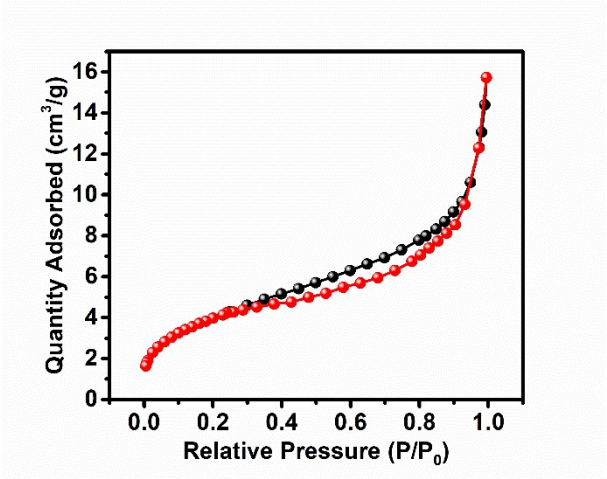

Figure S7. N_2 adsorption-desorption isotherms of SNFs-ZIF hybrid membrane.

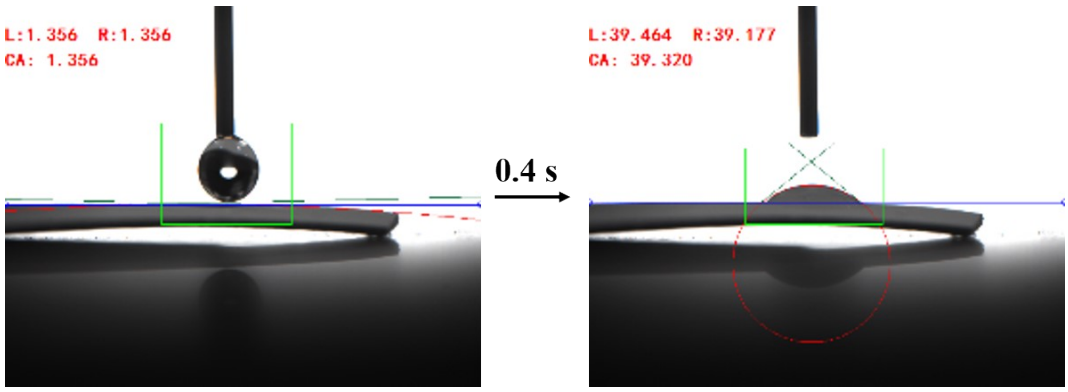

Figure S8. Water contact angle of SNFs-ZIF hybrid membrane.

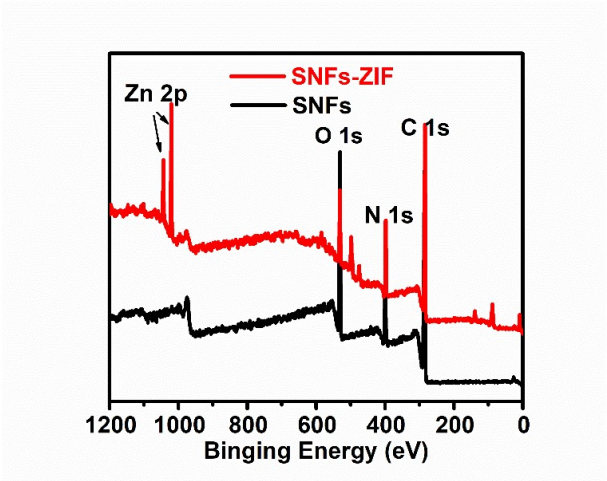

Figure S9. The full XPS spectrum of the SNFs (blank) and the SNFs-ZIF membrane (red). The characteristic peaks of Zn 2p appear in the SNFs-ZIF spectrum, further verifying the successful preparation of SNFs-ZIF.[1]

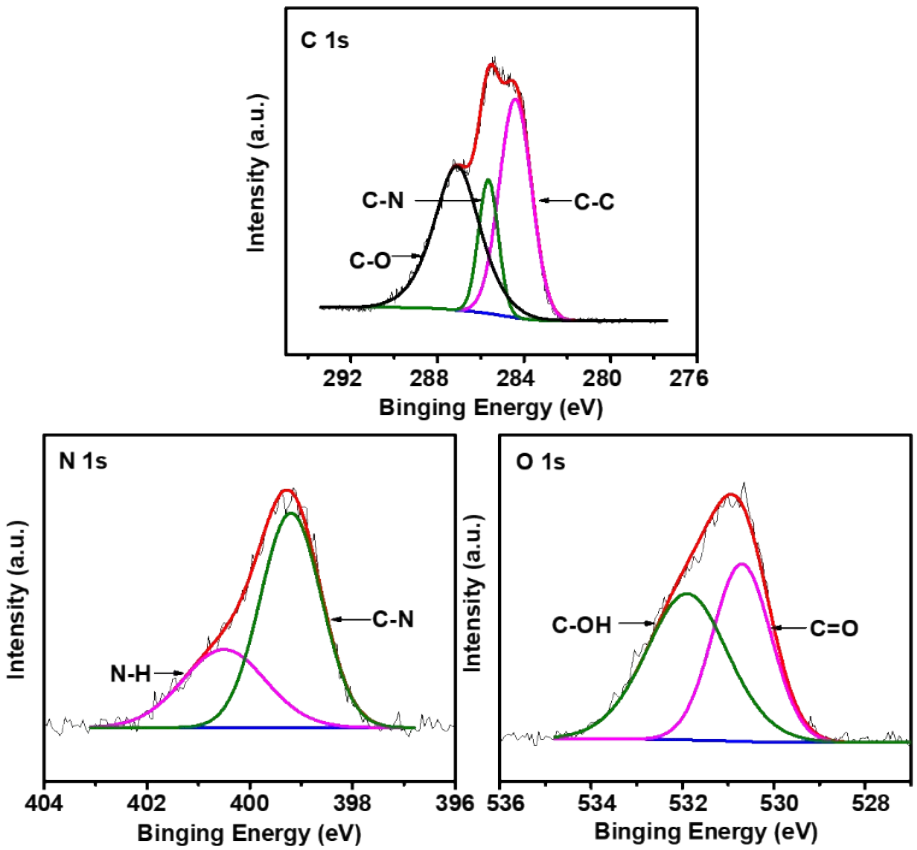

Figure S10. The high-resolution spectra of C, O, and N in SNFs. N 1s is fitted to two peaks, namely C–N and N–H are significant characteristic peaks at 399.2 eV and 400.5 eV, respectively. O 1s is also fitted to two peaks, located at 531.9eV (C–O) and 530.7eV (C=O).[2]

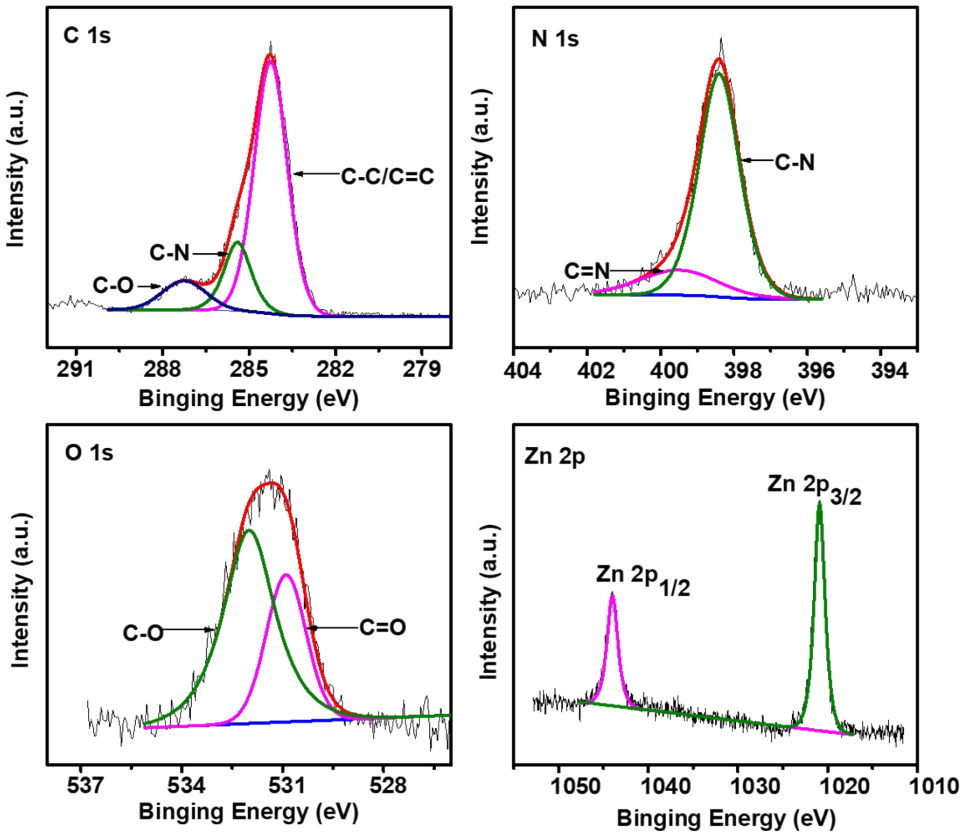

Figure S11. XPS spectrum fitting of the SNFs-ZIF hybrid membrane. The N 1s XPS spectrum give two peaks, centered around 399.5 eV and 398.4 eV, corresponding to C=N in 2-methyl-imidazole and C–N, respectively. The O 1s peak is deconvoluted into two peaks at 532.2 eV and 530.9 eV, which were attributed to C–O and C=O, respectively. While the Zn $2p_{3/2}$and $2p_{1/2}$ peaks locate at 1020.9 eV and 1044.1eV, showing consistence with previous reports.[1, 2]

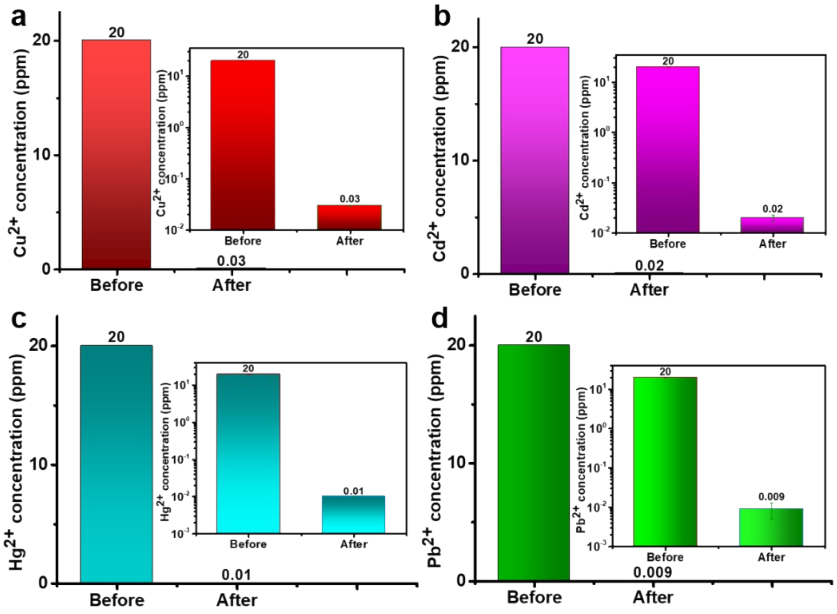

Figure S12. The concentration changes before and after filtration via the SNFs-ZIF membrane. Inner illustration: more intuitive demonstration of magnitude order after Cu^{2+} (a), Cd^{2+} (b), Hg^{2+} (c), and Pb^{2+} (d) were filtered.

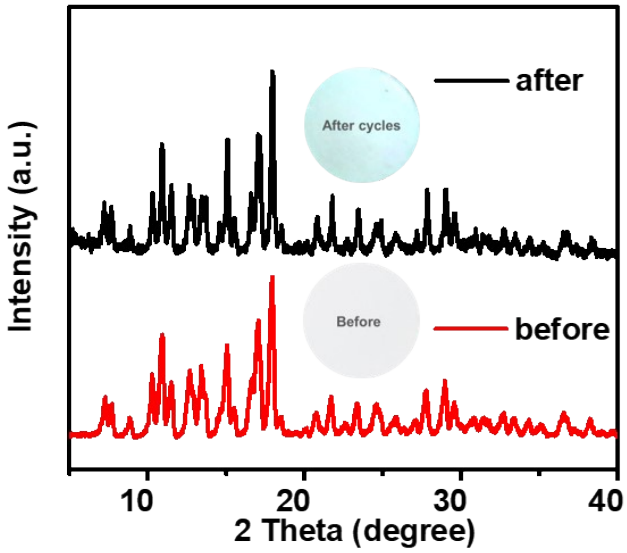

Figure S13. XRD spectra after the cycle and before the filtration. Inset: Digital photos of membrane before and after circulating filtration.

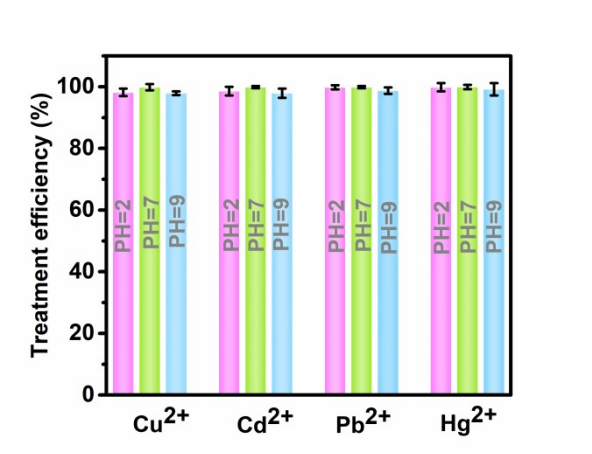

Figure S14. Treatment efficiency of the SNFs-ZIF hybrid membrane on four kinds of heavy metal ions (20 ppm, 30 mL) under different pH conditions. Different pH was regulated by 1M HNO_3 and 1M NaOH.

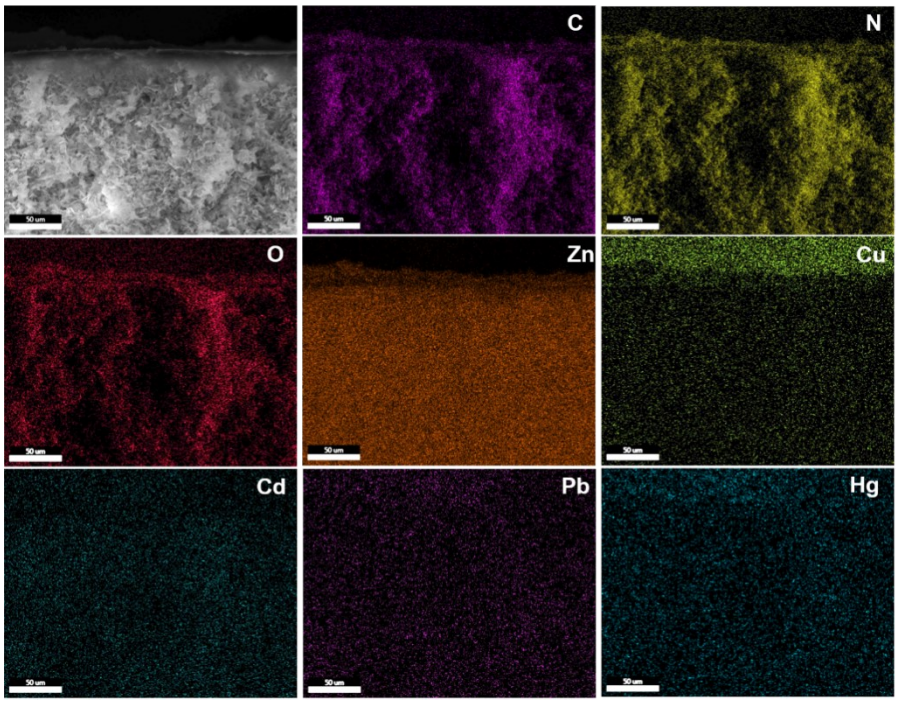

Figure S15. EDX mapping of the elemental distribution.

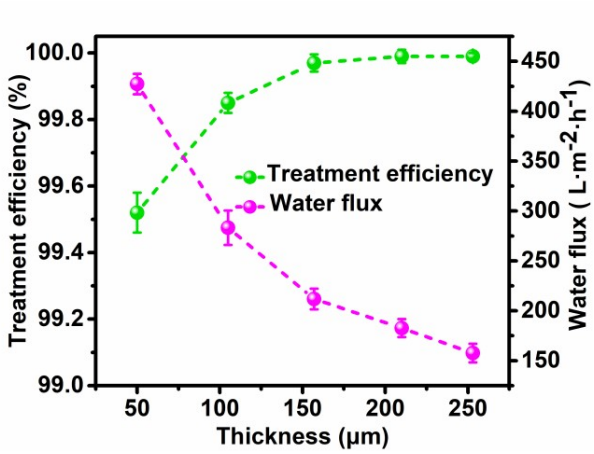

Figure S16. The effect of membrane thickness on the treatment efficiency and flow rate. The results indicated that with the increase of film thickness, the treatment efficiency of the film on copper ions increases to over 99.9%, and then tended to be stable. As expected, the membrane flux decreased with the increase of membrane thickness. Considering the water flow rate and treatment efficiency, the thickness of 105 μm is the best choice with the treatment efficiency of 99.85% and the flux of 354.06 $L \cdot m^{-2} \cdot h^{-1} \cdot bar^{-1}$.

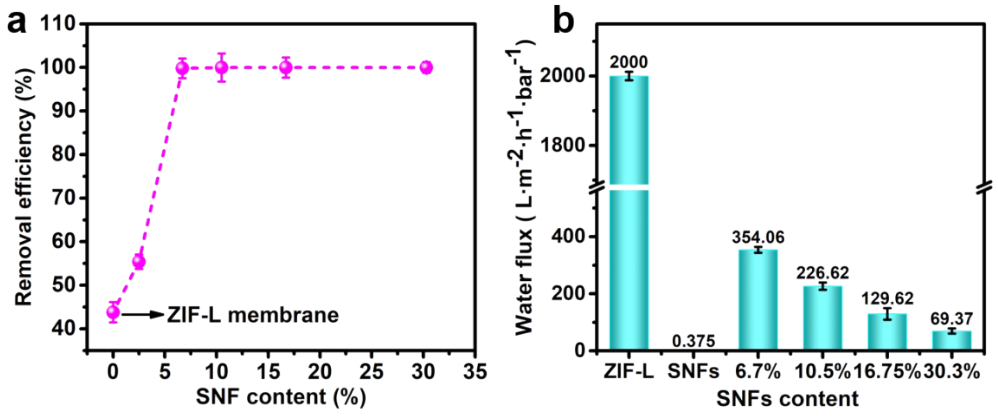

Figure S17. Under different SNFs content, the treatment efficiency (a) and water flux (b) of membrane for the removal of Cu^{2+} in wastewater.

Contaminant Adsorption experiments

Cu^{2+} sorption kinetics. Adsorption kinetic was performed at 25 °C. 10 mg SNFs-ZIF composite (SNFs: 6.7wt%) was added to a 100 mL beaker, which included 50 mL aqueous solution of Cu^{2+} (20 $mg \cdot L^{-1}$). The mixture was shaken for 2 hours. The supernatant was taken out at different specific time periods and filtered. The concentration of Cu^{2+} in aqueous solution was analyzed by ICP-MS. The distribution coefficient K_d is an important parameter to measure the performance of the adsorbents. The value of K_d can be determined by formula (1):

$$K_d = (C_i - C_f)/C_f \times (V/m) \quad (1)$$

where C_i indicates the initial concentration of the contaminant ($mg \cdot L^{-1}$), C_f indicates the final equilibrium concentration of the contaminant ($mg \cdot L^{-1}$), m is the mass of the adsorbent (g), and V is the volume of the tested liquid (mL).

The adsorbed amount for Cu^{2+} (q_t) was determined by the below equation (2):

$$q_t = (C_0 - C_t)/m \times V \quad (2)$$

where C_0 and C_t are the concentration of the Cu^{2+} ($mg \cdot L^{-1}$) initially and at time t, respectively, V is the volume solution used (L), and m is the mass of SNFs-ZIF (g).

Mathematical Models. The adsorption kinetics of pseudo-first-order rate equation and pseudo-second-order rate equation was used to investigate the adsorption process. The adsorption kinetic equations are given as Eq (3) and Eq (4), respectively.

$$\text{Log}\ (q_e - q_t) = \log q_e - k_1 t \quad (3)$$

$$t/q_t = 1/(k_2 q_e^2) + t/q_e \quad (4)$$

where q_e and q_t are the amount of Cu^{2+} adsorbed at equilibrium and time t (min), and k_1 (min^{-1}) and k_2 ($g \cdot mg^{-1} \cdot min^{-1}$) are the rate constant of the pseudo-first-order adsorption and the pseudo-second-order rate constant, respectively.[3]

Cu^{2+} adsorption isotherm. The adsorption isotherm of Langmuir and Freundlich models was used to further understand the adsorption mechanism. The adsorption isotherm equations are given as Eq (5) and Eq (6), respectively.

$$C_e/q_e = 1/(k_L q_m) + C_e/q_m \quad (5)$$

$$\log q_e = \log K_f + (1/n) \log C_e \quad (6)$$

where q_e and q_m represent the equilibrium and the maximum adsorption capacity ($mg \cdot g^{-1}$), respectively. Here, C_e is the Cu^{2+} concentration ($mg \cdot L^{-1}$) at equilibrium, and K_L ($L \cdot mg^{-1}$) is the Langmuir constant. Also, K_f ($L \cdot mg^{-1}$) and n are the Freundlich parameters related to adsorption capacity and adsorption intensity, respectively.[4]

According to the above equations, conclusions can be drawn that:

(1) The K_d values of the SNFs-ZIF hybrid membrane for Cu^{2+} can reach 2.28×10^5 $mL \cdot g^{-1}$.

(2) The pseudo-second-order rate model and the Langmuir model were selected as the adsorption kinetic and the adsorption isotherm between Cu^{2+} and SNFs-ZIF composite.

(3) The adsorbed capacity of SNFs-ZIF for Cu^{2+} attained 294 $mg \cdot g^{-1}$.

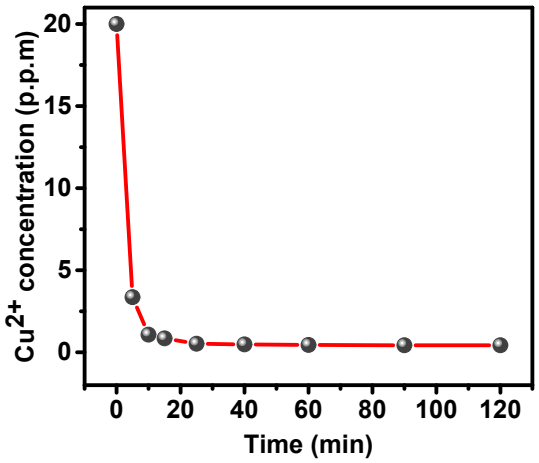

Figure S18. The concentration of Cu^{2+} in the solution decreased from 20 $mg \cdot L^{-1}$ to 0.85 $mg \cdot L^{-1}$ within 15 minutes when the membrane was used as adsorbent.

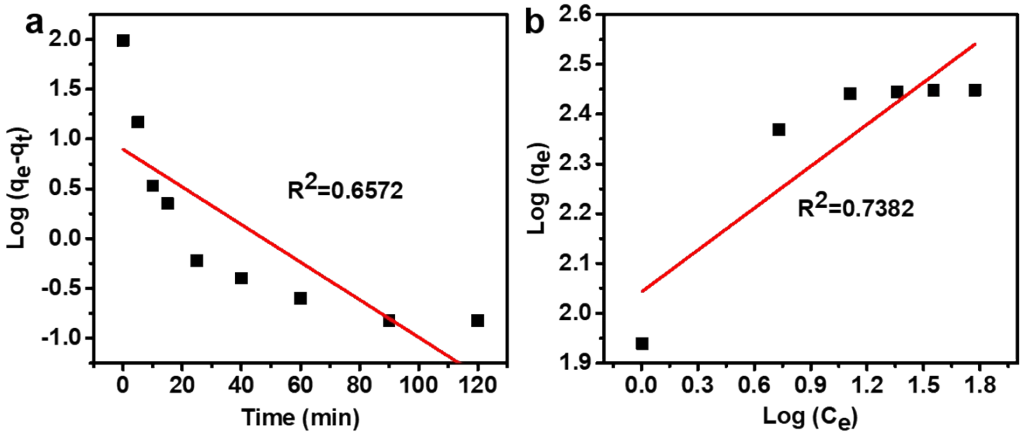

Figure S19. (a) Pseudo-first-order kinetic plot and (b) Freundlich isotherms for the adsorption mechanism between Cu^{2+} and SNFs-ZIF composite membranes (Cu^{2+} concentration: 20 $mg \cdot L^{-1}$).

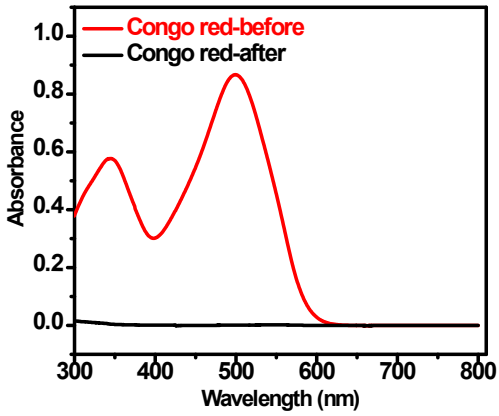

Figure S20. UV-visible spectra of 50 ppm (10 mL) Congo red solution before and after the treatment of SNFs-ZIF membrane.

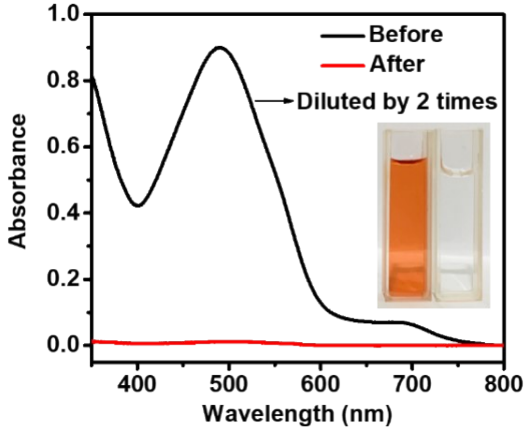

Figure S21. UV-visible spectra of 20 mL (each dyes concentration: 20 ppm) mixed solution filtered by SNFs-ZIF hybrid membranes.

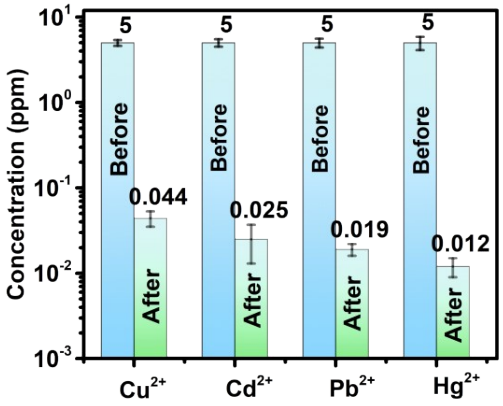

Figure S22. Concentration changes of multiple heavy metal ions in the mixed solution (co-existence of dyes and metal ions) before and after the filtration of SNFs-ZIF hybrid membranes.

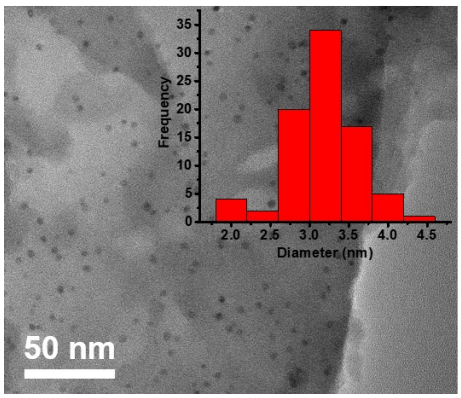

Figure S23. TEM images of Pd/CM, exhibiting the clearly visible Pd NPs on the carbonized SNFs-ZIF membrane substrate, after thermal reduction and cooling, and most of them are distributed in 2~3nm.Inset: size distribution of Pd nanoparticles.

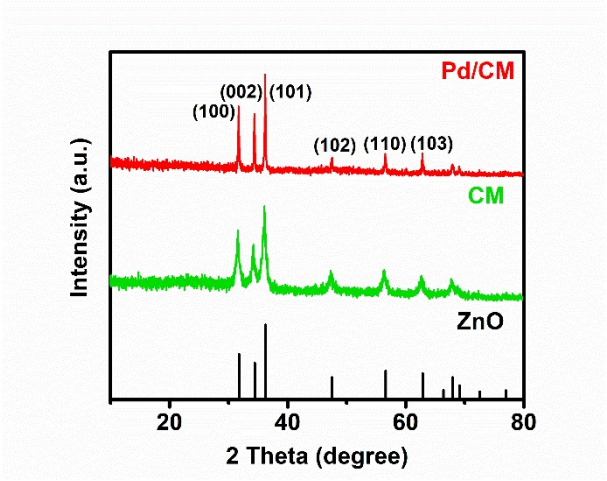

Figure S24. XRD spectra of the composite. Six typical diffraction peaks at 2θ of 31.77°, 34.42°, 36.25°, 47.53°, and 56.60°, 62.86° for the composite are indexed to (100), (002), (101), (102), (110) and (103) planes of ZnO (JCPDS 36-1451) crystal structure.[5]

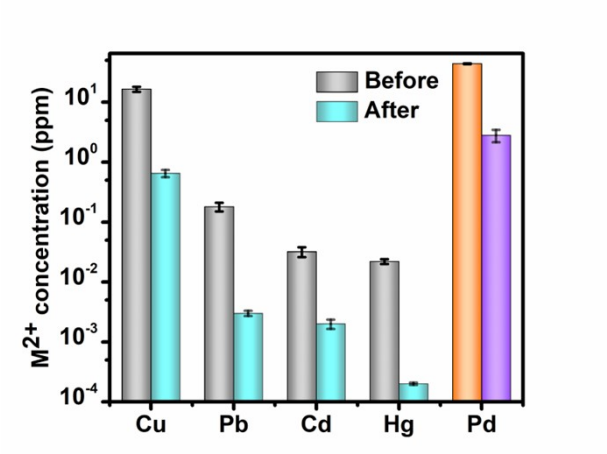

Figure S25. Concentration changes of multiple heavy metal ions and Pd^{2+} in actual wastewater before and after the filtration of SNFs-ZIF hybrid membranes.

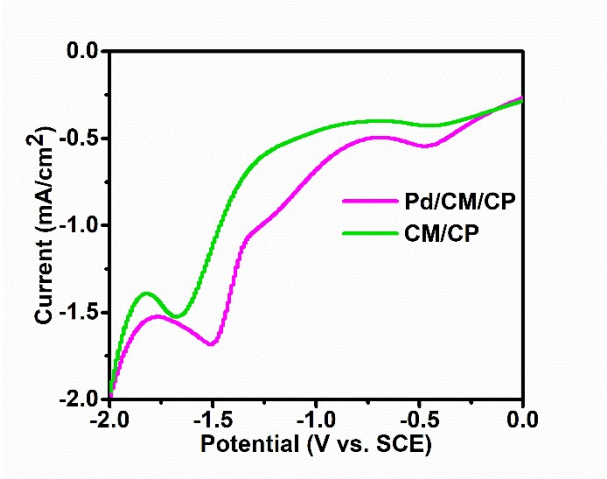

Figure S26. LSV curves on different cathodes. LSV tests at 2 $mV \cdot s^{-1}$ scan rate were set in a potential ranging from −2.0 V (vs. SCE) to 2.0 V (vs. SCE).

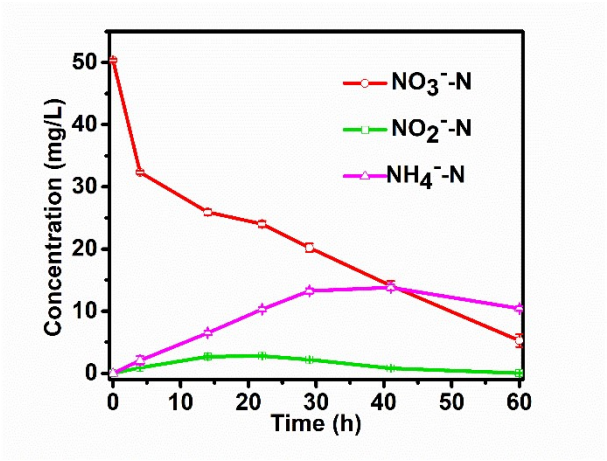

Figure S27. Time-variation concentrations of nitrate, nitrite, and ammonium ions. Experimental conditions: 50 $mg \cdot L^{-1}$ NO_3^--N, 0.05 $mol \cdot L^{-1}$ Na_2SO_4, −1.3 V (vs. SCE) of applied potential, 60 h.

Table S1. Performance comparison with reported relevant membrane.

Membrane material	Water permeance ($L \cdot m^{-2} \cdot h^{-1} \cdot bar^{-1}$)	Feed system	Rejection (%)	Ref.
Poly(ionic liquid)/PSF NF	7.55	Co^{2+}	85.2	6
		Cu^{2+}	84.9	
		Ni^{2+}	88.4	
Poly(ethyleneimine)/poly(dopamine)-MWCNTs/trimesoyl chloride NC NF	15.32	Zn^{2+}	93	7
		Cu^{2+}	90.5	
		Ca^{2+}	90.5	
Polydopamine functionalized halloysite nanotube-polyetherimide MMM	22.5	Pb^{2+}	78.5	8
		Cd^{2+}	75.6	
Polyimide TFC FO	2.4	Pb^{2+}	99.4	9
		Cd^{2+}	99.9	
		Cu^{2+}	99.8	
		Hg^{2+}	99.8	
ZIF-300	39.2	Cu^{2+}	99.21	10
		Cd^{2+}	99.32	

$ZnAl_2O_4$-TiO_2	5.1	Cd^{2+}	93	11
ultrafiltration		Pb^{2+}	93.4	
membranes		Cr^{2+}	96	
Poly(piperazineamide)	80	Pb^{2+}	＞99	12
thin film		Cd^{2+}	97	
		Co^{2+}	96	
		Cu^{2+}	99	
SNFs-ZIF membrane	354.1	Cu^{2+}	99.85	**This work**
		Cd^{2+}	≈100	
		Pb^{2+}	99.94	
		Hg^{2+}	99.92	

Table S2. Physicochemical properties of three dyes.

Name	Molecular formula	Molecular weight	Electricity
Condo red	$C_{32}H_{22}N_6Na_2S_2$	696	negative
Rhodamine B	$C_{28}H_{31}ClN_2O_3$	479	positive
Methylene blue	$C_{16}H_{18}ClN_3S$	319	positive

Table S3. Estimated total cost for preparing 1 g adsorbents.

Adsorbent	Materials	Amount used	Unit cost $	Cost $	Total cost $/g	Other costs	Ref.
TEMPO oxidized CNC	CNC	1 g	0.3	0.3	**2.8**	Dialyzing cellulose dialysis membrane for 1 week	13
	TEMPO-reagent	0.059 g	0.57	0.33			
	NaBr	0.325 g	0.112	0.04			
	NaClO	7.1 mL	0.19	1.35			
	Methanol	11 mL	0.063	0.7			
	NaOH	N/A mL	0.008	N/A			
	HCl	N/A mL	0.01	N/A			
DNPH modified γ-Al2O3	Alumina nanoparticles	2.0 g	9.175	18.35	**9.4**		14
	SDS	0.1 g	1.62	0.16			
	2,4-dinitroph-enylhydrazine	0.9	1.572	1.41			
ZnO	$Zn(CH_3COO)_2•2H_2O$	0.66 g	12.88	8.5	**82.55**	Heating at 160 ℃ for 12 h	15
	Urea	0.54 g	0.1542	0.08			
	Ethylene glycol	25 mL	0.432	10.8			
MWCNT	/	/	/	/	**42.35**		Sigma-

							Aldrich
SWCNT	/	/	/	/	**676**		Sigma-Aldrich
Graphene oxide	/	/	/	/	**2215**		Sigma-Aldrich
SNF/HAP	Cocoons	1 g	0.015	0.02	**1.1**	Degumming and dialysis	16
	LiBr	8.077 g	0.12	0.97			
	$CaCl_2$	0.133 g	0.343	0.05			
	Na_2HPO_4	0.17 g	0.39	0.07			
MOF-808/PAN	1,3,5-Benzenetricarboxylic acid	0.7860 g	1.159	0.911	> **80.99**		17
	$ZrOCl_2 \cdot 8H_2O$	1.209 g	14.32	17.31			
	PAN	0.5 g	4.3	2.15			
	DMF	160 mL	0.152	24.32			
	Anhydrous formic acid	150 mL	0.166	24.9			
	EDTA-2Na	18.60 g	2.817	52.39			
	Organic solvents	/	/	/			
SNFs-ZIF	Cocoons	1 g	0.04	0.44	**1.98**	Degumming and	**This work**
	LiBr	3.23 g	0.067	0.216			

$Zn(NO_3)_2 \cdot 6H_2O$	0.168 g	4.551	0.764	dialysis
2-methylimidazole	0.26 g	0.321	0.08	

Reference

(1) Q. Huo, J. Li, X. Qi, G. Liu, X. Zhang, B. Zhang, Y. Ning, Y. Fu, J. Liu and S. Liu, Cu, Zn-embedded MOF-derived bimetallic porous carbon for adsorption desulfurization. *Chem. Eng. J.*, 2019, **378**, 122106.

(2) L. Zhou, N. Li, G. Owens and Z. Chen, Simultaneous removal of mixed contaminants, copper and norfloxacin, from aqueous solution by ZIF-8. *Chem. Eng. J.*, 2019, **362**, 628-637.

(3) R. Guo, X. Cai, H. Liu, Z. Yang, Y. Meng, F. Chen, Y. Li and B. Wang, In Situ Growth of Metal-Organic Frameworks in Three-Dimensional Aligned Lumen Arrays of Wood for Rapid and Highly Efficient Organic Pollutant Removal. *Environ. Sci. Technol.*, 2019, **53**, 2705-2712.

(4) I. Andjelkovic, D. N. Tran, S. Kabiri, S. Azari, M. Markovic and D. Losic, Graphene Aerogels Decorated with alpha-FeOOH Nanoparticles for Efficient Adsorption of Arsenic from Contaminated Waters. *ACS Appl. Mater. Interfaces*, 2015, **7**, 9758-9766.

(5) M. T. Efa and T. Imae, Hybridization of carbon-dots with ZnO nanoparticles of different sizes. *J. Taiwan Inst. Chem. Eng.*, 2018, **92**, 112-117.

(6) Y. Tang, B. Tang and P. Wu, Preparation of a positively charged nanofiltration membrane based on hydrophilic–hydrophobic transformation of a poly(ionic liquid). *J. Mater. Chem. A*, 2015, **3**, 12367-12376.

(7) F. Y. Zhao, Y. L. Ji, X. D. Weng, Y. F. Mi, C. C. Ye, Q. F. An and C. J. Gao, High-Flux Positively Charged Nanocomposite Nanofiltration Membranes Filled with Poly(dopamine) Modified Multiwall Carbon Nanotubes. *ACS Appl. Mater. Interfaces*, 2016, **8**, 6693-6700.

(8) R. S. Hebbar, A. M. Isloor, K. Ananda and A. F. Ismail, Fabrication of polydopamine functionalized halloysite nanotube/polyetherimide membranes for heavy metal removal. *J. Mater. Chem. A*, 2016, **4**, 764-774.

(9) Y. Cui, Q. Ge, X.-Y. Liu and T.-S. Chung, Novel forward osmosis process to effectively remove

heavy metal ions. *J. Membr. Sci.*, 2014, **467**, 188-194.

(10) J. Yuan, W.-S. Hung, H. Zhu, K. Guan, Y. Ji, Y. Mao, G. Liu, K.-R. Lee and W. Jin, Fabrication of ZIF-300 membrane and its application for efficient removal of heavy metal ions from wastewater. *J. Membr. Sci.*, 2019, **572**, 20-27.

(11) N. Saffaj, H. Loukili, S. Alami Younssi, A. Albizane, M. Bouhria, M. Persin and A. Larbot, Filtration of solution containing heavy metals and dyes by means of ultrafiltration membranes deposited on support made of Moroccan clay. *Desalination* 2004, **168**, 301-306.

(12) A. Bera, J. S. Trivedi, S. B. Kumar, A. K. S. Chandel, S. Haldar and S. K. Jewrajka, Anti-organic fouling and anti-biofouling poly(piperazineamide) thin film nanocomposite membranes for low pressure removal of heavy metal ions. *J. Hazard. Mater.*, 2018, **343**, 86-97.

(13) S. Hokkanen, A. Bhatnagar and M. Sillanpaa, A review on modification methods to cellulose-based adsorbents to improve adsorption capacity. *Water Res.*, 2016, **91**, 156-173.

(14) X. Pu, Z. Jiang, B. Hu and H. Wang, γ-MPTMS modified nanometer-sized alumina micro-column separation and preconcentration of trace amounts of Hg, Cu, Au and Pd in biological, environmental and geological samples and their determination by inductively coupled plasma mass spectrometry. *J. Anal. At. Spectrom.*, 2004, **19**, 984-989. (15) X. Wang, W. Cai, Y. Lin, G. Wang and C. Liang, *J. Mater. Chem.*, 2010, **20**. 8582–8590.

(16) S. J. Ling, G. Qin, W. W. Huang, S.F. Cao, D. L. Kaplan and Markus B. J., Design and function of biomimetic multilayer water purification membranes. *Sci. Adv.*, 2017, **3**, 1-11.

(17) X. Chen, D. Chen, N. Li, Q. Xu, H. Li, J. He and J. Lu, Modified-MOF-808-Loaded Polyacrylonitrile Membrane for Highly Efficient, Simultaneous Emulsion Separation and Heavy Metal Ion Removal.*ACS Appl. Mater. Interfaces*, 2020, **12**, 39227-39235.